PCCP

Experimental determination of the temperature dependence of the absolute rate coefficients of the HCCO + NO_2 and HCCO + H_2 reactions

S. A. Carl,* Q. Sun, L. Teugels and J. Peeters

Department of Chemistry, University of Leuven, Celestijnenlaan 200F, B-3001, Leuven, Belgium. E-mail: Shaun.Carl@chem.kuleuven.ac.be

Received 22nd September 2003, Accepted 20th October 2003
First published as an Advance Article on the web 10th November 2003

The absolute rate coefficients of the gas-phase reactions HCCO + NO_2 and HCCO + H_2 were experimentally determined for the first time over extended temperature ranges: 293 K to 769 K and 438 K to 761 K, respectively. HCCO radicals were generated by pulsed-laser photolysis of CH_2CO at 193 nm. Their subsequent decay, under pseudo-first-order conditions, was monitored in real-time using a laser-photofragment/laser-induced fluorescence technique. The rate coefficient of HCCO + NO_2 exhibits a negative temperature dependence similar to that of the HCCO + NO reaction, but the Arrhenius A-factor is 1.4 times larger; $k(T)_{(HCCO+NO_2)} = (2.3 \pm 0.4) \times 10^{-11}$ exp (340 ± 40) K/T) cm^3 s^{-1}. It is argued that, if the major product channels yield N, NH or NCO, the HCCO + NO_2 reaction should be a significant removal route of NO_x in stationary combustion systems under fuel-rich conditions at temperatures below *ca.* 1300 K. The rate coefficient for the HCCO + H_2 reaction was determined as $k(T)_{(HCCO+H_2)} = (2.2 \pm 1.4) \times 10^{-11}$ exp(-2000 ± 400)K/T). In fuel-rich combustion environments, given the high concentrations of H_2, this reaction is likely to be a significant loss process for HCCO radicals: $k(1500\ K)_{HCCO+H_2} = (6^{+0.4}_{-0.2}) \times 10^{-12}$ cm^{-3} s^{-1}, a factor of three greater than $k(1500\ K)_{HCCO+O_2}$.

1. Introduction

Recently the reactivity of HCCO has been the subject of several experimental and theoretical investigations that have gone some way in filling a prominent gap in our knowledge of the reactivity of small hydrocarbon radicals, especially in relation to hydrocarbon combustion and to NO_x-Reburning.

The HCCO radical was largely overlooked until clear evidence was forthcoming of it being the dominant product over a wide temperature range of the prominent $C_2H_2 + O$ reaction[1–3] indicating that the chemical flux through HCCO should be one of the largest of all small hydrocarbon radicals in hydrocarbon combustion under fuel-rich conditions, where C_2H_2 is ubiquitous.

$$C_2H_2 + O \rightarrow HCCO + H \quad (k_{1a}/k_1 \cong 0.8 : 285\ K \text{ to } 2100\ K) \tag{1a}$$

$$C_2H_2 + O \rightarrow CH_2 + CO \quad (k_{1b}/k_1 \cong 0.2 : 285\ K \text{ to } 2100\ K) \tag{1b}$$

Under these conditions high concentrations of CH_3 radicals are generated causing the CH_3 self-reaction to dominate $CH_3 + O$. The former initiates the chemistry of species containing two carbon atoms, leading to C_2H_2 and HCCO, whilst the latter reaction is largely connected to the chemistry of species containing a single carbon atom.[4]

Subsequent reactions of HCCO have been shown to generate $CH_2(^1A_1)$[1] and hence CH radicals[5] and can therefore be linked directly and indirectly to the production of ultra-violet[6] and visible[7,8] chemiluminescence, soot,[9–11] chemi-ions,[12,13] 'prompt' CO_2[14,15] and 'prompt' NO.[16]

HCCO also participates significantly in the removal of NO_x in NO_x-reburning strategies[17–20] in which nitric oxide formed in stationary combustion systems is removed by small hydrocarbon radicals (HCCO, CH_3, CH, $CH_2(^3B_1)$, $CH_2(^1A_1)$, or C_2H or C) generated from a hydrocarbon added in a second combustion stage under fuel-rich conditions. Removal of NO begins by reaction with a small carbon-containing radical. Several intermediate steps yield NH_i species ($i = 0$ to 2), NCO or N_2O. Further reaction of NH_i and NCO with NO and reaction of N_2O with H, as well as decomposition of N_2O, leads finally to N_2. The main reactions[20–23] of the "natural" Re-burning scheme are given in Fig. 1.

Since the review by Carl *et al.*[24] on the limited number of direct experiments on HCCO reactivity, several other studies have been published. The major products of the reaction of HCCO with O_2 have been determined experimentally[14] and theoretically.[15] In the latter theoretical study the overall rate constant was also calculated by variational transition-state theory; however, in order to obtain agreement of the magnitude and temperature dependence of the calculated rate constants with the earlier experimental determinations[1,24] the calculated barrier height had to be reduced from 19 kJ mol^{-1} to only 5 kJ mol^{-1}.

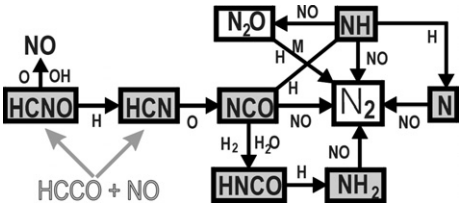

Fig. 1 The main reactions involved in the natural reburning scheme. The important HCCO + NO reburning reaction yields HCN and HCNO as products. The large number of products available to HCCO + NO_2 appear in the shaded boxes. For most potential products of the HCCO + NO_2 reaction only one additional step is required to give N_2.

 DOI: 10.1039/b311684k

The absolute rate coefficient of HCCO + NO has been determined by Carl *et al.* over the temperature range 296 K to 802 K.[25] Both the magnitude and the temperature dependence of the rate constant were reproduced by the theoretical work of Tokmakov *et al.*[26] The experimental product-distributions[27–29] have also been confirmed theoretically.[26,30] The combination of the experimental rate constant of Carl *et al.*[25] and the latest theoretical, *T*-dependent product distribution study of Tokmakov *et al.*[26] shows that the HCCO + NO reaction should have a smaller contribution to "natural" NO-reburning than previously modelled.[20,31] This contribution may still be important provided that a substantial fraction of the major product, HCNO, is converted to HCN *via* reaction with H (Fig. 1). Thus, better characterisation of NO_x reburning requires a closer examination of other potential reburning reactions that could compete with HCCO + NO.

Of concern to the present investigation are the reactions HCCO + NO_2 and HCCO + H_2, at elevated temperatures. The former reaction may be influential in NO-reburning, whilst the latter, if it has a sufficiently large rate constant, may constitute a significant loss process for HCCO given the relatively large concentrations of H_2 in fuel-rich hydrocarbon combustion.

In stationary-source hydrocarbon combustion, a large fraction of NO_x is in the form of NO so that reactions of small hydrocarbon radicals with this species usually dominate their NO_2 counterparts, particularly at high temperatures. The degree of participation of NO_2 in NO_x flame chemistry depends largely on the temperature-sensitive $[NO_2]/[NO]$, which is controlled mainly by the reactions $NO + HO_2 \rightarrow NO_2 + OH$, $NO_2 + H \rightarrow NO + OH$, $NO + H + M \rightarrow HNO + M$ and $HNO + H \rightarrow NO + H_2$.[32] These reactions usually dictate that concentrations of NO_2 are significant at temperatures below about 1400 K. Thus in low-temperature and fuel-rich conditions — as typical in NO_x-reburning — radical reactions involving NO_2 are expected to contribute to the overall NO_x chemistry. Furthermore, the HCCO + NO_2 reaction may take on added importance as a reburning reaction because several of its possible reaction channels yield NCO, NH, or N-atoms. These products lie at the heart of the reburning scheme, as shown in the shaded boxes of Fig. 1. The thermochemically possible product channels of HCCO + NO_2 are given below.

		$\Delta_r H(298\ \mathrm{K})/\mathrm{kJmol^{-1}}$
HCCO + NO_2		
→ COOH + N + CO	(2a)	−69
→ HCO + N + CO_2	(2b)	−88
→ (HOCN, HNCO) + O + CO	(2c, d)	−97, −194
→ NCO + OH + CO	(2e)	−121
→ NO + CO + CO + H	(2f)	−121
→ CN + OH + CO_2	(2*g*)	−128
→ (HNC, HCN) + O_2 + CO	(2h, i)	−129, −184
→ (HNC, HCN) + O + CO_2	(2j, k)	−163, −218
→ COOH + NCO	(2l)	−273
→ NH + CO_2 + CO	(2m)	−360
→ (HONC, HCNO, HOCN, HNCO) + CO_2	(2n, o, p, q)	−386, −426, −629, −726

An enthalpy of formation, $\Delta_f H$(298 K), for HCCO of 176 kJ mol^{-1}[33] was used in the calculation of the above reaction enthalpies. If channels (2a) or (2b) are important, HCCO + NO_2 could be a major source of N atoms below 1400 K.

So far, the only experimental data of the rate constant of reaction (2) is the single-temperature determination by Temps *et al.*[34] who reported k_2 (298 K) = $(2.7 \pm 0.7) \times 10^{-11}$ cm^3 s^{-1}.

There have been no reported direct measurements of the HCCO + H_2 reaction, and it is largely ignored in kinetic models involving HCCO. Yet, several exothermic product channels are open to this reaction:

			$\Delta_r H(298\ \mathrm{K})/\mathrm{kJmol^{-1}}$
HCCO + H_2	→ CH_2CO + H	(3a)	−6
	→ CH=CHOH	(3b)	−61
	→ CH_3 + CO	(3c)	−140
	→ CH_2CHO	(3d)	−163
	→ CH_3CO	(3e)	−200

which is therefore a potentially significant sink for HCCO in fuel-rich hydrocarbon flames.

2. Experimental method

As the experimental apparatus, experimental procedure and our detection method for HCCO has been described in detail on a previous occasion,[24] only the principal points are repeated here.

The stainless-steel reaction chamber is O-ring sealed at both ends by water-cooled quartz windows that allow access for two pulsed photolysis laser beams and a pulsed probe laser beam.

A 3-cm in diameter ceramic tube (99.7% Al_2O_3, with an internal, gray, oxidized SiC coating) inside the reaction chamber, surrounded by a Ni/Cr resistive wire, allows the gas mixture to be heated to temperatures up to 900 K. The laser beams enter and exit the ceramic tube, at right angles to its axis, *via* opposite 1.5-cm diameter holes in the tube. The temperature of the gas in the small probed reaction volume—where the photolysis beam crosses the Al_2O_3 tube—is monitored using a movable, calibrated chromel/alumel thermocouple. Spreads in the gas temperature range from ±1 K at 296 K to ±10 K at 769 K, our highest-temperature kinetic measurements.

A third window, at right angles to the axis of the collinear laser beams, and facing the mouth of the Al_2O_3 tube, allows imaging of fluorescence from the reaction volume.

The reaction chamber is connected to a throttled, rotary vacuum pump and a gas flow system allowing fresh, homogeneous gas mixtures of constant total pressure (typically 5.0 Torr) and known composition to continually pass. The gas mixture comprises ketene as the photolytic precursor of HCCO, the co-reactant NO_2 (2.5% in ultra high purity He, Air Products) or H_2 (99.995% purity, L'Air Liquide), and He (99.999% purity, Indugas). Using long-path absorption, the NO_2 fraction in the NO_2/He mixture was verified to be $(2.47 \pm 0.06) \times 10^{-2}$. The gases are admitted to the flow system from their high-pressure cylinders *via* calibrated flow controllers (MKS Instruments Inc.). Ketene is produced *in situ*, upstream of the reaction chamber, using a method similar to that employed by Unfried *et al.*,[35] *i.e.* by pyrolysis of diketene vapour (the liquid phase of 98% purity is stabilised by copper sulfate, Aldrich Chemical Corporation) in He at 800 K. A 195 K (acetone/dry ice) trap situated immediately downstream of the pyrolysis tube is used to collect any undissociated diketene before the gas enters the reaction chamber. The typical concentration of ketene in the reaction chamber is about 5×10^{15} molecule cm^{-3}.

Co-reactant concentrations, $[NO_2]$ (or $[H_2]$), are accurately determined using partial flow rates, measured using calibrated mass flow controllers (MKS Instruments inc.), and total reactor pressure, measured using a 0 to 10 Torr Barocel pressure sensor (Datametrics). Total flow rates through the reactor are typically 150 sccm (cm^3 min^{-1} at STP), which is sufficiently fast to replenish the gas in the reaction volume in the 0.1 s period between successive excimer laser pulses, but still slow

enough for the gas to be effectively static over the HCCO 1/e-lifetimes, which range from 7–100 μs.

HCCO radicals are generated by pulsed laser (ArF excimer laser,193 nm, *ca.* 20 mJ pulse^{-1} at 10 Hz, beam area = 3 cm^2) photolysis of ketene along the central axis of a heatable, stainless-steel reaction chamber.

$$CH_2CO + 193\ nm \rightarrow HCCO\ (\tilde{X}^2A'' \text{ and/or } \tilde{A}^2A') + H(^1S) \quad (k_{6a}/k_6 = 0.11) \quad (4a)$$

$$CH_2CO + 193\ nm \rightarrow CH_2\ (\tilde{a}^1A_1) + CO \quad (k_{6b}/k_6 = 0.19) \quad (4b)$$

$$CH_2CO + 193\ nm \rightarrow CH_2(\tilde{X}^3B_1) + CO \quad (k_{6c}/k_6 = 0.63) \quad (4c)$$

$$CH_2CO + 193\ nm \rightarrow C_2O\ (\tilde{b}^1\Sigma^+) + H_2 \quad (k_{6d}/k_6 = 0.07) \quad (4d)$$

The indicated branching ratios are those of ref. 36.

After HCCO generation *via* process (4a), time-resolved measurement of the [HCCO] decay is achieved using a novel ''laser-photofragment/laser-induced fluorescence'' technique (LPF-LIF), in which a first probe laser pulse (266 nm) photo-dissociates HCCO yielding CH(X, $N'' = 1$ to 28) + CO and a second probe laser pulse (*ca.* 430 nm), delayed by only a few nanoseconds, excites the (A ← X) transition in a highly rotationally-excited ($N'' = 13$ or 15) CH photofragment, thus inducing CH-fluorescence the intenstiy of which is proportional to [HCCO].[24] Our recent work[24] demonstrates that nascent CH photo-fragments resulting from the photolysis of HCCO at 266 nm exhibit a highly-excited rotational population distribution (up to $N'' = 28$) and are therefore easily distinguished from any chemically-produced CH, which possess a Boltzmann rotational distribution with a population maximum at $N'' = 3$ at 298 K and $N'' = 5$ at 800 K. Therefore, the wavelength of the CH(A ← X) probe laser pulse is tuned to a Q-branch transition originating from a specific highly-rotationally-excited state ($N'' = 13$ or $N'' = 15$, depending on the reactor temperature):

$$CH(X\ ^2\Pi,\ \nu'' = 0,\ N'' = 13 \text{ or } 15) + h\nu(430.35 \text{ nm or } 430.00 \text{ nm}) \rightarrow CH(A\ ^2\Delta,\ \nu' = 0,\ N' = 13 \text{ or } 15) \quad (5a)$$

$$CH(A\ ^2\Delta) \rightarrow CH(X\ ^2\Pi) + h\nu(ca.\ 430\ nm) \quad (5b)$$

Probe laser absorption from thermally populated $N'' = 13$ and 15 levels of CH(X) produced by chemical reaction, is negligible under our experimental conditions below reactor temperatures of *ca.* 600 K and 1000 K, respectively. Nevertheless, effective discrimination of photo-fragment CH radicals requires that the time delay between (4) and (5a) be sufficiently short to avoid rotational relaxation of the high-N'' levels. Such a short time delay, of *ca.* 16 ns, is achieved simply by introducing an optical path difference of 5 m between the HCCO photolysis pulse (Nd : YAG 4ω, 10 Hz) and the CH fragment excitation pulse (Nd : YAG/Dye; *ca.* 430 nm, 10 Hz).

The intensity of the 193 nm photolysis beam was about 7 mJ cm^{-2} per pulse. The fraction of ketene, lying along the laser path, dissociated to HCCO is calculated to 6×10^{-4}, based on a molecular absorption cross-section[37] of σ(ketene at 193 nm) = 8×10^{-19} cm^2 and a quantum yield for dissociation to HCCO of 0.11.[36] In the presence of a large excess [NO_2] ($33 < [NO_2]/[HCCO] < 600$) or [H_2] ($260 < [H_2]/[HCCO] < 2300$), the [HCCO] decays obey pseudo-first-order kinetics with reaction 1/e lifetimes ranging from about 7 μs to 100 μs. Note also that at our experimental pressure of 5 Torr (He), the two Renner–Teller states of HCCO are expected to be always equilibrated; in 10 μs, an HCCO radical undergoes about a thousand collisions with the He bath gas.

NO_2 is also known to dissociate at 193 nm. According to a recent study by Sun *et al.*,[38] photolysis at 193 nm of NO_2 has two dissociation channels:

$$NO_2 + h\nu(193\ nm) \rightarrow O(^3P) + NO \quad (6a)$$

$$NO_2 + h\nu(193\ nm) \rightarrow O(^1D) + NO \quad (6b)$$

with a branching fraction, k_{6b}/k_6, of 0.55 ± 0.03. In the same study the room temperature rate constant for $O(^1D) + NO_2$ was determined as $(1.5 \pm 0.3) \times 10^{-10}$ cm^{-3} s^{-1} and the absorption cross-section of NO_2 at 193 nm was estimated to be $(2.9 \pm 1.2) \times 10^{-19}$ cm^{-2}. Under our experimental conditions, a fraction of *ca.* 2×10^{-3} of [NO_2] should thus be photolysed. The possible influence of side reactions of HCCO with photolysis products of NO_2 and CH_2CO, as well as that of secondary chemistry is discussed in the next section.

Optical emissions {CH(A ← X)} from the centre of the reaction chamber pass through the third window and are imaged onto a photomultiplier tube (PMT) (R955, Hamamatsu) fitted with a band-pass filter (430 nm ± 10 nm (FWHH), Oriel 59295). The PMT photo-current, resulting from the transient CH fluorescence, is voltage-converted and passed to a boxcar for integration (SR250, Stanford Research Systems, gate width = 1.0 μs). The integrated signal for a given gate delay, is collected as a single data point on computer using a 12-bit A/D converter (ADC-12, PICO Technology Limited).

Exponential decay profiles of $[HCCO]_t$ are collected pulse-wise and constructed over a few minutes by incrementing the time delay between the excimer laser pulse and the HCCO probe beam pulses after each excimer laser pulse. It is important that the observed emission intensity should remain proportional to $[HCCO]_t$ whilst the decay signal is being constructed. Thus in order to minimise any possible drifts in the I_{obs}/[HCCO] ratio due, for example, to a slight wavelength drift of the CH(X → A) probe laser pulse—a drift of 0.001 nm is sufficient to cause a 15% change in signal intensity—the whole 100–500 μs decay time-range is scanned rapidly in a few seconds. This is repeated several times and all decay profiles are summed until the signal-to-noise ratio is sufficiently high. This method of data acquisition is much more desirable than employing a single, slower scan with an equal total number of data points, which would be much more influenced by a wavelength drift.

Triggering and precision timing (to 0.1 μs resolution) of the excimer and Nd : YAG fundamental pulses, as well as the Boxcar gate, is accomplished using a computer-controlled pulse generator (National Instruments NOI 3066). In previous experiments[24,25] very strong emission from CH(A) (1/e-lifetime of *ca.* 540 ns[39]) produced directly by two-photon photolysis of ketene at 193 nm interfered with that from CH(A) produced by HCCO photolysis at 266 nm by overdriving the PMT such that signal linearity was recovered only after *ca.* 15–20 μs. Thus [HCCO] time profiles could only be reliably collected after this time.

$$CH_2CO + 2h\nu(193\ nm) \rightarrow CH(A^2\Delta) + \text{products} \quad (7)$$

$$CH(A\ ^2\Delta) \rightarrow CH(X\ ^2\Pi) + h\nu(ca.\ 430\ nm) \quad (5b)$$

We have since incorporated a home-built gating system to the PMT that reverses the voltage applied between the 2nd and the 3rd dynode preventing amplification of the electron beam for the duration of the interfering CH(A) emission (*ca.* 2 μs) enabling us now to reliably collect HCCO time profiles beginning at *ca.* 4 μs.

3. Results and discussions

In the presence of an excess concentration of NO_2 or H_2 the time profile of [HCCO] should take the following simple

exponential form:

$$[\mathrm{HCCO}]_t/[\mathrm{HCCO}]_0 = \exp(-k_2[\mathrm{NO_2}] - \Sigma_i(k_i[R_i])t) \quad \text{(i)}$$

where the summation represents removal rate of HCCO by all side and secondary reactions involving radical species R_i, having a rate constant k_i. A similar equation, with $k_3[\mathrm{H_2}]$ instead of $k_2[\mathrm{NO_2}]$ applies in the presence of H_2 as co-reactant. Diffusion out of the observation region at the pressures and temperatures of the experiments is negligibly slow compared to reactive removal.

For our experiments with NO_2 as co-reactant, the first (constant) term of the argument of the exponential function dwarfs the second term, which describes mainly the reaction of HCCO with (time-varying concentrations of) H-atoms that are produced in the photolysis of CH_2CO. For experiments with H_2 as co-reactant the second term represents a significant fraction of the overall decay. In the absence of co-reactant the time profiles showed nearly exponential behaviour, indicating that the second term of the exponential remains nearly constant over the observed decay time, thus a fit to a single exponential function is valid. In earlier experiments[24] with a telescoped excimer beam, a pronounced second-order component in the [HCCO] decay profiles was observed, which was probably due to higher densities of radicals being produced by the larger photon flux.

3.1 HCCO + NO_2

Fig. 2 shows typical time profiles of [HCCO] in the presence of excess $[NO_2]$ at 358 K obtained from (430 ± 10) nm LIF of nascent (266 nm) photofragment CH following its initial excitation at 430.35 nm (from $N'' = 13$). All decays, measured in the presence of NO_2, exhibit the expected exponential behaviour described by eqn. (i) over the whole signal range of typically two orders of magnitude (see Fig. 2).

The resulting first-order rate constants, as given by the slopes of the $\ln[\mathrm{HCCO}]_t$ *versus* t plots, are plotted in Fig. 3 as a function of $[NO_2]$ for three representative experimental temperatures. A weighted, least-squares linear fit to the data gives the rate constant k_2. The experimental determinations of k_2 at all the various T are listed in Table 1. Also included in Table 1 are the k_2 determinations for two experiments carried out at different total pressure to the rest: one at 2.0 Torr, the other at 10.0 Torr. These results, taken with the other k_2 determinations at 5.0 Torr show the HCCO + NO_2 reaction to be independent of pressure. The low intercepts of the k'-*versus*-$[NO_2]$ plots of Fig. 3 (*ca.* 5×10^3 s^{-1}) relative to the maximum k' values (of 0.5×10^5 s^{-1} to 1.6×10^5 s^{-1}) demonstrate the dominance of the HCCO + NO_2 reaction over

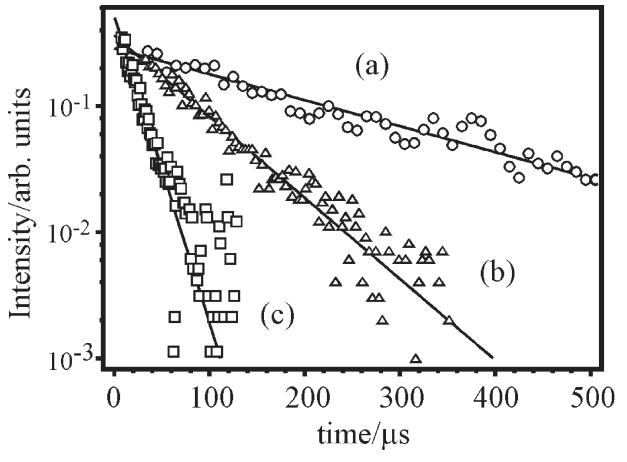

Fig. 2 Examples of time profiles of HCCO following pulsed laser production from CH_2CO at 358 K. $[CH_2CO]_{initial} = 5 \times 10^{15}$ cm^3, $P_{total} = 5.0$ Torr. (a) $[NO_2] = 0$ cm^{-3}, (b) $[NO_2] = 1.0 \times 10^{14}$ cm^{-3}, (c) $[NO_2] = 8.2 \times 10^{14}$ cm^{-3}.

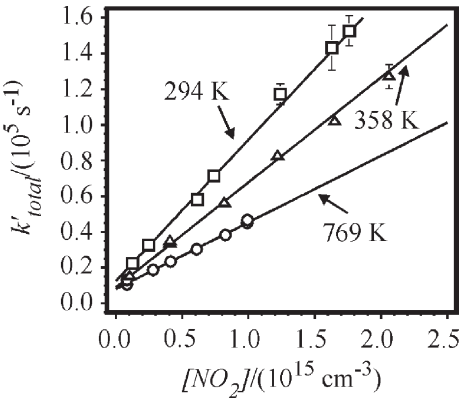

Fig. 3 Second-order plots of pseudo-first-order decay rate *vs.* $[NO_2]$ at three different temperatures. The gradient of the fits (solid line) gives k_2.

reactions of HCCO with radicals produced by photolysis of CH_2CO [reaction (4)]. Secondary reactions arising from the addition of NO_2 also have a negligible influence on the HCCO time profile under our experimental conditions.

Photolysis of CH_2CO generates HCCO and H, together with larger amounts of $CH_2(^3B_1)$ (also by fast quenching of $CH_2(^1A_1)$). Reaction of HCCO with all these radicals, R_i, cause [HCCO] to decay (with $[NO_2] = 0$ cm^{-3}) at a rate of $(5 \pm 2) \times 10^3$ s^{-1}: the intercept values of the plots in Fig. 3. For an initial $\Sigma[R_i]$ of 5.5×10^{-3} $[CH_2CO]$ at a laser fluence of 7 mJ cm^{-2} per pulse and $\sigma = 8 \times 10^{-19}$ cm^2, this implies an average R_i + HCCO rate coefficient of *ca.* $(1.8 \pm 0.7) \times 10^{-10}$ cm^3 s^{-1}, which is a reasonable value. Generally, reactions of the added NO_2 with the R_i (*i.e.* CH_2, HCCO and H) will form other radicals, R'_i, while the total concentration of the radicals remains roughly constant. As the rate coefficients $k(R_i + \mathrm{HCCO})$ and $k(R'_i + \mathrm{HCCO})$ are expected to differ by no more than 1×10^{-10} cm^3 s^{-1}, the maximum change in the $\Sigma k_i[R_i]$ is expected to be $\leq 3 \times 10^3$ s^{-1}. This is $\leq 3\%$ of the observed total change of k' by NO_2 addition, which is of the order of 10^5 s^{-1}.

The influence of both $O(^3P)$ and $O(^1D)$ produced in process (6a) on HCCO decay profiles is also negligible compared to that of NO_2 as the $[O]/[NO_2]$ ratio is only 2×10^{-3}, and the rate constant ratio, k_O/k_{NO_2}, is at most 5. Moreover, the O-atoms react fairly rapidly with NO_2. Thus, the O-atom contributes less than 1% to the HCCO removal by NO_2 addition.

All determined rate constants, k_2, are displayed in Arrhenius form in Fig. 4. A weighted least-squares fit to the data

Table 1 Experimental absolute rate constants for the reaction HCCO + NO_2 at various temperatures. $P_{tot} = 5.0$ Torr, He bath gas

Reactor temperature/K	$k_2/10^{-11}$/cm^3 s^{-1}
293	7.6 ± 1.0
294	7.9 ± 0.6
294	7.8 ± 0.8
294	7.6 ± 0.8
294[a]	8.0 ± 0.4
294[b]	8.3 ± 0.8
323	7.8 ± 0.2
358	5.9 ± 0.2
393	4.9 ± 0.4
407	5.6 ± 0.4
453	4.8 ± 0.2
605	4.1 ± 0.2
690	4.0 ± 0.4
769	3.7 ± 0.4

[a] $P_{tot} = 2.0$ Torr. [b] $P_{tot} = 10.0$ Torr.

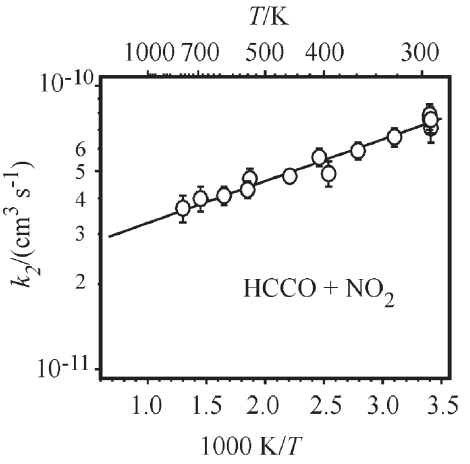

Fig. 4 Experimental rate constants for $HCCO + NO_2$ as a function of temperature plotted in Arrhenius form. The results are fitted by a weighted, least-squares, analysis to a simple Arrhenius expression, yielding $k_2(T) = (2.3 \pm 0.4) \times 10^{-11}$ exp (340 ± 40) K$/T$) cm^3 s^{-1}.

gives $k_2(T) = (2.3 \pm 0.4) \times 10^{-11}$ exp (340 ± 40) K$/T$) cm^3 s^{-1}. The negative temperature dependence observed for this reaction—very similar to that found for $HCCO + NO$[25,26]—is not at all unusual for a rapid barrier-less reaction between free radicals. A common explanation[40] is related to increased preference with increasing temperature of the initially-formed reaction complex to re-traverse the reaction path to reactants over the loose (variational) transition state of the entrance channel. According to the theoretical work of Lin and co-workers[41,42] this situation accounts entirely for the strong negative temperature dependence of the reaction $NCO + NO$.[43]

Our recent theoretical work on the characterisation of the $HCCO + NO$ potential energy surface though shows that at temperatures up to about 700 K re-dissociation should be very small.[30] A gradual tightening of the variational entrance-channel transition state as the temperature is increased may therefore be the dominant cause of the decrease in the $HCCO + NO$ rate constant over this temperature range. A similar effect could account for the temperature dependence observed for $HCCO + NO_2$. To what degree re-dissociation plays a role in the $HCCO + NO_2$ reaction in the temperature range covered here is uncertain without reference to a detailed potential energy surface. According to Tokmakov *et al.*,[26] the total rate constant for the $HCCO + NO$ reaction drops off very rapidly above 800 K due to an increasing fraction of re-dissociation. The possibility of a similar behaviour of the $HCCO + NO_2$ reaction means that rate constants extrapolated from the present experimental data to combustion temperatures (above *ca.* 1400 K) should be considered as an upper limit.

The average value of all our room-temperature data is $(7.9 \pm 0.8) \times 10^{-11}$ cm^3 s^{-1}, almost a factor of three greater than that determined by Temps *et al.*[34] There are similar discrepancies also between our $HCCO + O_2$ and $HCCO + NO$ rate constants at room temperature and those found by Temps *et al.*[34] The reasons for these discrepancies are not clear. Our $HCCO + O_2$ and $HCCO + NO$ rate constants compare favourably with those of the earlier experimental studies of other groups[35,44] and for $HCCO + NO$ with a later theoretical study from another group.[26]

HCCO + H_2

The time-resolved data for the $HCCO + H_2$ reaction are of a quality similar to those recorded for the $HCCO + NO_2$ reaction with decays following a single exponential profile over *ca.* two orders of magnitude: examples are given in Fig. 5.

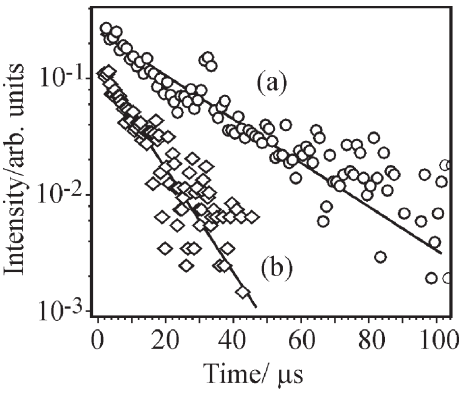

Fig. 5 Examples of time profiles of HCCO following pulsed laser production from CH_2CO at 751 K. $[CH_2CO]_{initial} = 3 \times 10^{15}$ cm^3, $P_{total} = 5.0$ Torr. (a) $[H_2] = 0$ cm^{-3}, (b) $[H_2] = 3.7 \times 10^{15}$ cm^{-3}.

The derived k's *vs.* $[H_2]$ for a selection of temperatures are displayed in Fig. 6, the gradients of these plots yielding k_3.

Here, unlike the $HCCO + NO_2$ experiments, the change in total removal rate of HCCO on addition of the co-reactant (H_2) is smaller than, or similar to, the intercept value, the latter being due to removal of HCCO by radical species produced in the photolysis of CH_2CO. This suggests also a possible influence of secondary chemistry on the removal of HCCO if reaction (3) yields species that are highly reactive toward HCCO. Note that the other photo-product of ketene, $CH_2(X\ ^3B_1)$, reacts only very slowly with H_2 at our T-range.[45] According to the possible product channels of reaction (3), this secondary removal of HCCO could be with H atoms. Since $CH_2(X)$ is present in concentrations almost an order-of-magnitude larger than those of HCCO[36] and that $H + HCCO$ and $CH_2 + H$ reactions have rate constants of similar magnitude (*ca.* 1.5×10^{-10} cm^3 s^{-1}), it is expected that of any H-atoms formed in reaction (3) less than 20% will react with HCCO (allowing for a factor-of-two uncertainty in the HCCO branching ratio obtained in ref. 36) as the majority of the rest will react will $CH_2(X)$. Thus for about every five reactions of HCCO with H_2 there is at most only one subsequent HCCO reaction with H-atoms formed in reaction (3). This situation would result in a maximum overestimation of the rate constant, k_3, of 20% (our quoted errors in k_3 are 2σ statistical errors derived from fits of k' *vs.* $[H_2]$ and do not include this possible systematic bias (Table 2), which is added later). Having said that, there is theoretical evidence that the H-atom yield in the $HCCO + H_2$ reaction is only small. The $[H_3C_2O]$ potential energy surface has been explored by Ding *et al.*[46] in their theoretical study of the $C_2H + H_2O$ reaction. Though in that study no direct connection could be found between

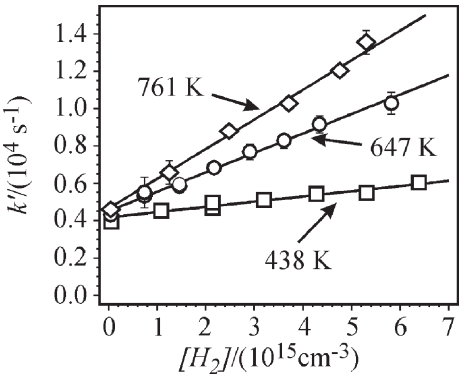

Fig. 6 Second-order plots of pseudo-first-order decay rate *vs.* $[H_2]$ at three different temperatures. The gradient of the fits (solid line) gives k_3.

Table 2 Experimental absolute rate constants for the reaction $HCCO + H_2$ at various temperatures. $P_{tot} = 5.0$ Torr, He bath gas

Reactor temperature/K	$k_3/10^{-13}/cm^3\ s^{-1}$
438	2.8 ± 1.0
546	5.2 ± 1.2
606	8.3 ± 3.6
647	10 ± 2.0
702	14 ± 2.6
761	16 ± 3.4

$C_2H + H_2O$ and lower-lying $HCCO + H_2$, the authors did calculate a barrier of 49 kJ mol^{-1} for reaction channel (3a), $HCCO + H_2 \rightarrow CH_2CO + H$. This barrier is much larger than the activation energy of 16.6 kJ mol^{-1} derived from this study for the overall reaction (3).

The Arrhenius plot for $HCCO + H_2$ is shown in Fig. 7. A weighted least-squares fit to all our data gives $k_3(T) = (2.2 \pm 1.4) \times 10^{-11}\ \exp(-2000 \pm 400)K/T)\ cm^{-3}\ s^{-1}$. Because of the limited $1/T$ range of the data the co-variance of the two-parameter fit was also determined to aid extrapolation to higher temperatures: it is equal to $7.41 \times 10^{-5}\ cm^{-3}\ s^{-1}$ K. From this co-variance and the other fit parameters 95% confidence limits of the Arrhenius fit were determined. To the upper confidence limit a factor $0.2k_3(T)$ was added to approximately take into account the (one-sided) systematic error mentioned above. As can be seen from extrapolation of the Arrhenius plot, the rate constant becomes significant even at moderate combustion temperatures, approaching $1 \times 10^{-11}\ cm^3\ s^{-1}$ at 2000 K. It is therefore expected to be a significant removal route for HCCO in H_2-rich combustion environments.

Conclusions

The absolute rate constant of $HCCO + NO_2$ has been, for the first time, experimentally determined over an extended temperature range. To compare the potential of this reaction in reburning to that of the $HCCO + NO$ reaction we use the rate constant of the "reburning" channel $HCCO + NO \rightarrow HCN + CO_2$ of $2 \times 10^{-12}\ cm^3\ s^{-1}$ in the 1200–1300 K temperature range[24,30] and a total rate constant of $3 \times 10^{-11}\ cm^{-3}\ s^{-1}$ for $HCCO + NO_2$ over the same temperature. The

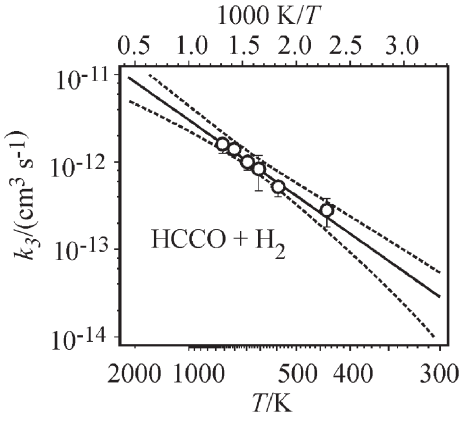

Fig. 7 Experimental rate constants for $HCCO + H_2$ as a function of temperature plotted in Arrhenius form. The results are fitted (solid line) by a weighted, least-squares analysis to a simple Arrhenius expression, yielding $k_3(T) = (2.2 \pm 1.4) \times 10^{-11}\ \exp(-2000 \pm 400)K/T))\ cm^3\ s^{-1}$. The dashed lines represent 95% confidence limits that were constructed using the covariance (see text). They are asymmetrically distributed about the best fit to take into account the possible $+0.2k_3(T)$ systematic error in the data.

$[NO]/[NO_2]$ fraction under typical reburning conditions[47] is expected to be *ca.* 1000 at 1300 K and *ca.* 100 at 1200 K—though these values could vary considerably as they depend on the precise combustion conditions. If we take these figures as a guide and assume that (a) only the HCN channel of $HCCO + NO$ reaction participates in reburning and (b) the most important reaction channels in the $HCCO + NO_2$ reaction give NCO, NH or N, then the contribution to NO_x reburning of the $HCCO + NO_2$ reaction compared to the $HCCO + NO$ reaction should be at least 2% at 1300 K and at least 20% at 1200 K. Certainly at temperatures higher than 1400 K the $HCCO + NO_2$ reaction can be neglected.

We have also presented the first determination of the rate constants of the $HCCO + H_2$ reaction. Extrapolation of the present experimental results show that the rate constant is large at moderate to high combustion temperatures ($k > 5 \times 10^{-12}\ cm^3\ s^{-1}$). Above 1400 K this reaction should be an important removal route for HCCO and should therefore be included in future modelling studies where HCCO kinetics have a significant impact. At 1400 K the rate constant, k_3, is predicted to be $5 \times 10^{-12}\ cm^3\ s^{-1}$. Again, adopting values of typical reburning conditions[47] with an average mole fraction of H_2 in the 10^{-3} to 10^{-2} range, it can be shown that the rates of reaction of HCCO with H_2 should be similar to those of HCCO with NO during the removal of NO, at an initial NO mole fraction of 10^{-3}.

The reaction of $HCCO + H_2$ is expected to dominate that of $HCCO + O_2$ ($k_{(HCCO+O_2)}$ at 1400 K is *ca.* $2 \times 10^{-12}\ cm^3\ s^{-1}$[24]) under fuel-rich conditions owing to the very large H_2 concentration relative to that of O_2.

Acknowledgements

The authors gratefully acknowledge support of the Fund for Scientific Research, Flanders (FWO-Vlaanderen), for a post-doctoral mandate (S. A. C) and a research project, and the KULeuven Research Council (BOF Fund) for continuing support, including a PhD grant (Q. S). We thank Dr P. Dagaut for providing us with some results of detailed kinetic modelling computations relating to NO_x reburning by natural gas.

References

1 (*a*) J. Peeters, M. Schaekers and C. Vinckier, *J. Phys. Chem.*, 1986, **90**, 6552; (*b*) W. Boullart and J. Peeters, *J. Phys. Chem.*, 1992, **96**, 9810.
2 P. Frank, K. A. Bhaskaran and Th. Just, *Symp. (Int.) Combust., [Proc.]*, 1986, **21**, 885.
3 J. V. Michael and A. F. Wagner, *J. Phys. Chem.*, 1990, **94**, 2453.
4 J. Warnatz, *Symp. (Int.) Combust.. [Proc.]*, 1992, **24**, 553 and references therein.
5 K. H. Homann and H. Schweinfurth, *Ber Bunsen-Ges. Phys. Chem.*, 1981, **85**, 569.
6 J. Grebe and K. H. Homann, *Ber. Bunsen-Ges. Phys. Chem.*, 1982, **86**, 581.
7 J. Grebe and K. H. Homann, *Ber. Bunsen-Ges. Phys. Chem.*, 1982, **86**, 587.
8 K. Devriendt and J. Peeters, *J. Phys. Chem. A*, 1997, **101**, 2546.
9 J. Peeters and K. Devriendt, *Symp. (Int.) Combust., [Proc.]*, 1996, **26**, 1001.
10 N. M. Marinov, W. J. Pitz, C. K. Westbrook, M. J. Castaldi and S. M. Senkan, *Combust. Sci. Technol.*, 1996, **21**, 116.
11 C. S. McEnally and L. D. Pfefferle, *Combust. Flame*, 2000, **121**, 575.
12 J. Peeters, W. Boullart and K. Devriendt, *J. Phys. Chem.*, 1995, **99**, 3583.
13 D. E. Phippen and K. D. Bayes, *Chem. Phys. Lett.*, 1989, **164**, 625.
14 D. L. Osborn, *J. Phys. Chem. A*, 2003, **107**, 3728.
15 S. J. Klippenstein, J. A Miller and L. B. Harding, *Symp. (Int.) Combust., [Proc.]*, 2003, **29**, 1209.

16 J. Blauwens, B. Smets and J. Peeters, *Symp. (Int.) Combust., [Proc.]*, 1976, **16**, 1055.
17 J. O. L. Wendt, C. V. Sterling and M. A. Matovich, *Symp. (Int.) Combust., [Proc.]*, 1973, **14**, 897.
18 W. Boullart, M. T. Nguyen and J. Peeters, *J. Phys. Chem.*, 1994, **98**, 8036.
19 P. Kilpinen, P. Glarborg and M. Hupa, *Ind. Eng. Chem. Res.*, 1992, **31**, 1477.
20 P. Dagaut, J. Luche and M. Cathonnet, *Int. J. Chem. Kinet.*, 2000, **32**, 365.
21 P. Dagaut, F. Lecomte, S. Chevailler and M. Cathonnet, *Combust. Flame*, 1999, **119**, 494.
22 C. T. Bowman, *Symp. (Int.) Combust., [Proc.]*, 1992, **24**, 859.
23 P. Glarborg, M. U. Alzueta, K. Dam-Johansen and J. A. Miller, *Combust. Flame*, 1998, **115**, 1.
24 S. A. Carl, Q. Sun and J. Peeters, *J. Chem. Phys.*, 2000, **114**, 10 332.
25 S. A. Carl, Q. Sun, L. Vereecken and J. Peeters, *J. Phys. Chem A*, 2002, **106**, 12 242.
26 I. V. Tokmakov, L. V. Moskaleva, D. V. Paschenko and M. C. Lin, *J. Phys. Chem. A*, 2003, **107**, 1066.
27 W. Boullart, M. T. Nguyen and J. Peeters, *J. Phys. Chem.*, 1994, **98**, 8036.
28 U. Eickhoff and F. Temps, *Phys. Chem. Chem. Phys.*, 1999, **1**, 243.
29 K. T. Rim and J. F. Hershberger, *J. Phys. Chem. A*, 2000, **104**, 293.
30 L. Vereecken, R. Sumathy, S. A. Carl and J. Peeters, *Chem. Phys. Lett.*, 2001, **344**, 400.
31 P. Glarborg, M. U. Alzueta, K. Dam-Johansen and J. A. Miller, *Combust. Flame*, 1998, **115**, 1.
32 T. Faravelli, A. Frassoldati and E. Ranzi, *Combust. Flame*, 2003, **132**, 188.
33 D. L. Osborn, D. H. Mordaunt, H. Coi, R. T. Bise, D. M. Neumark and C. M. Rohlfing, *J. Chem. Phys.*, 1997, **106**, 10 087.
34 F. Temps, H. G. Wagner and M. Wolf, *Z. Phys. Chem. (Munich)*, 1992, **176**, 27.
35 K. G. Unfried, G. P. Glass and R. F. Curl, *Chem. Phys. Lett.*, 1991, **177**, 33.
36 G. P. Glass, S. S. Kumaran and J. V. Michael, *J. Phys. Chem. A*, 2000, **104**, 8360.
37 G. L. Vaghjiani, *Work-in-progress poster 4-D11*, 28th International Symposium on Combustion, Edinburgh, UK, 2000.
38 F. Sun, G. P. Glass and R. F. Curl, *Chem. Phys. Lett.*, 2001, **337**, 72.
39 J. Luque and D. Crosley, *J. Chem. Phys.*, 1996, **104**, 2146.
40 M. Mozurkewich and S. W. Benson, *J. Phys. Chem.*, 1984, **88**, 6429.
41 M. C. Lin, Y. He and C. F. Melius, *J. Phys. Chem.*, 1993, **97**, 9124.
42 R. Zhu and M. C. Lin, *J. Chem. Phys.*, 2000, **104**, 10 807.
43 D. Y. Juang, J.-S. Lee and N. S. Wang, *Int. J. Chem. Kinet.*, 1995, **27**, 1111.
44 K. K. Murray, K. G. Unfried, G. P. Glass and R. F. Curl, *Chem. Phys. Lett.*, 1992, **192**, 512.
45 D. C. Darwin and C. B. Moore, *J. Phys. Chem.*, 1995, **99**, 13 467.
46 Y. H. Ding, X. Zhang, Z. S. Li, X. R. Huong and C. C. Sun, *J. Phys. Chem. A*, 2001, **105**, 8215.
47 Personal communication, P. Dagaut. Model calculations are based on an initial fuel mixute of 7270 ppm $CH_4 + 728$ ppm C_2H_6 in the presence of an initial concentration 900 ppm NO. The equivalence ratio Φ was 1.5. $[NO_2]/[NO]$ ratios were taken after 120 ms. Detailed model results of similar calculations can be found in P. Dagaut, J. Luche and M. Cathonnet, *Int. J. Chem. Kinet.*, 2000, **32**, 365 and P. Dagaut, F. Lecomte, S. Chevailler and M. Cathonnet, *Combust. Flame*, 1999, **119**, 494.